Effect of Excess Li on the Structural and Electrical Properties of Garnet-Type $Li_6La_3Ta_{1.5}Y_{0.5}O_{12}$

Sumaletha Narayanan,[a] Gregory Thomas Hitz,[b,*] Eric D. Wachsman,[b,] and Venkataraman Thangadurai[a,***,z]**

[a]*Department of Chemistry, University of Calgary, Calgary T2N 1N4, Canada*
[b]*University of Maryland Energy Research Center, Department of Materials Science and Engineering, University of Maryland, College Park, Maryland 20742, USA*

Volatility of lithium during preparation of lithium-stuffed garnet-type metal oxide solid Li ion electrolytes is a common problem, which affects phase formation, ionic conductivity, mechanical strength and density. Synthesis of Li-stuffed garnets has been performed generally using the conventional solid-state reactions at elevated temperature in air. The present study describes the effect of excess $LiNO_3$ (2.5 to 15 wt.%) addition during the ceramic synthesis on the structural and electrical properties of garnet-type $Li_6La_3Ta_{1.5}Y_{0.5}O_{12}$. Powder X-ray diffraction (PXRD) confirmed that cubic phase was formed in all tested cases, and there is no significant variation in lattice parameter with amount of excess $LiNO_3$ used. However, increasing amounts of excess lithium decreased inter-particle contact and increased grain growth during sintering, producing sharply varied microstructures. PXRD showed no secondary phase and scanning electron microscopy (SEM) analysis showed rather uniform morphology and absence of "glassy" materials at the grain-boundaries. The bulk Li ion conductivity was found to increase with amount of excess lithium, reaching a maximum room temperature conductivity of 1.62×10^{-4} Scm^{-1} for the sample prepared using 10 wt.% excess $LiNO_3$. Raman microscopy study indicated the presence of Li_2CO_3 in all aged $Li_6La_3Ta_{1.5}Y_{0.5}O_{12}$ samples prepared using excess $LiNO_3$.
© The Author(s) 2015. Published by ECS. This is an open access article distributed under the terms of the Creative Commons Attribution Non-Commercial No Derivatives 4.0 License (CC BY-NC-ND, http://creativecommons.org/licenses/by-nc-nd/4.0/), which permits non-commercial reuse, distribution, and reproduction in any medium, provided the original work is not changed in any way and is properly cited. For permission for commercial reuse, please email: oa@electrochem.org. [DOI: 10.1149/2.0321509jes]
All rights reserved.

Manuscript submitted April 1, 2015; revised manuscript received May 11, 2015. Published June 17, 2015.

Li-stuffed garnet-type metal oxides have been considered as a potential candidate solid electrolyte material to replace conventional organic liquid based Li ion conducting electrolytes in Li-ion batteries, since members of garnet solid electrolytes exhibit high bulk ion conductivity of 10^{-4}-10^{-3} Scm^{-1} at room temperature. Furthermore, some of the garnet-type electrolytes show excellent chemical stability against reaction with elemental Li, Li-ion insertion or intercalation cathodes and high electrochemical stability window.[1,2] However, the synthesis of high bulk Li ion conducting garnet-type metal oxide-based lithium ion conductors is a challenging process, very sensitive to preparation conditions used, that are not yet fully characterized. For example, $Li_7La_3Zr_2O_{12}$ calcined at 1230°C results in highly conducting (7×10^{-4} Scm^{-1} at room temperature) cubic phase with a space group *Ia-3d* whereas a calcining temperature of 980°C leads to tetragonal phase with a space group $I4_1/acd$, which showed 2 orders of magnitude less conductive than cubic phase.[3,4] Traditional solid-state techniques are the most commonly used to synthesize garnet-type metal oxides, but usually require the highest sintering temperature resulting in the production of large particles.[5–8] It is known that volatilization of lithium occurs in the furnace, therefore, several researchers commonly compensate with a 10 wt.% excess lithium precursors.[3,9,10] Al-doped $Li_7La_3Zr_2O_{12}$ prepared without adding any excess lithium salts during synthesis, but varying the processing using powder cover condition for sintering, greatly affects the morphology, grain size and density.[11] Attempts have also been made to reduce the sintering temperature and improve the control of stoichiometry via wet chemical synthesis as well as through additives acting as sintering aids.[12–18]

It has been shown that Al migrates from the alumina crucible used for garnet synthesis, causing significant effects in the material including stabilization of the cubic phase.[15–18] Lithium salts such as Li_2O, Li_3BO_4, Li_3PO_4 and Li_4SiO_4 have been shown to significantly affect the electrical and microstructural properties.[13,18,19] Liu et al. showed that excess lithium (0 to 50 mol.%) added during synthesis of $Li_{6.5}La_3Ta_{0.5}Zr_{1.5}O_{12}$ increase the density and Li ion conductivity by the liquid phase formation during sintering.[19] This seems due to reaction between the excess lithium and aluminum impurity from the crucible, which was clearly visible from the PXRD studies. The optimization of Li_2O addition for $Li_{6.75}La_3Zr_{1.75}Ta_{0.25}O_{12}$ has been performed by Li et al. and found that 6 wt. % excess Li_2O is required for best conducting ceramic (6.4×10^{-4} Scm^{-1} at room temperature), which is about 3 times higher than that of $Li_{6.75}La_3Zr_{1.75}Ta_{0.25}O_{12}$ prepared without adding excess Li_2O.[20] They also found that the glassy-like phase formed at the grain-boundaries increases the density of material as well as helps to decrease the grain-boundary and improve the total Li^+ conductivity. Sakamoto group has explored high pressure and high temperature method to prepare dense garnet-type Li ion electrolytes and such a technique can be used to control the loss of Li content.[21] In the present study, we systematically investigate the effect of excess $LiNO_3$ (2.5 to 15 wt.%) on the structural, microstructural and Li ion conductivity properties of fast Li ion conducting garnet-type $Li_6La_3Ta_{1.5}Y_{0.5}O_{12}$ to understand the role of Li content and its optimization for high ionic conductivity.

Experimental

Synthesis of Li garnets.— Garnet-type $Li_6La_3Ta_{1.5}Y_{0.5}O_{12}$ oxide was prepared by solid-state (ceramic) method in air at elevated temperature. The precursors used were $LiNO_3$ (99%, Alfa Aesar), La_2O_3 (99.99%, Alfa Aesar) (pre-heated at 900°C for 24 h), Ta_2O_5 (99.5%, Alfa Aesar) and $Y(NO_3)_3$ (99.9%, Alfa Aesar). The amount of excess $LiNO_3$ added was varied between 2.5 and 15 wt.% in order to compensate for the lithium loss and to understand the role of excess Li ion phase formation, microstructure and Li ion conductivity. The synthesis process involved the conventional heating and ball milling steps. Pulverisette, Fritsch, Germany ball mill at a spinning rate of 200 rpm for 6 h using 2-propanol was used to ensure homogeneous mixing of the powder before and after the heating process at 700°C for 6 h. Pelletization was done using an isostatic press and the pellets were covered with mother powder in clean alumina crucible. Heating process involved 2 stages, 900°C for 24 h and a final sintering of 1100°C for 6 h in ambient air.

Phase, microstructure and conductivity characterization.— The powder X-ray diffraction (PXRD) was used to study the phase purity of samples using a Bruker D8 powder X-ray diffractometer with

*Electrochemical Society Student Member.
**Electrochemical Society Fellow.
***Electrochemical Society Active Member,
[z]E-mail: vthangad@ucalgary.ca

Downloaded on 2016-08-30 to IP 136.159.160.69 address. Redistribution subject to ECS terms of use (see ecsdl.org/site/terms_use) unless CC License in place (see abstract).

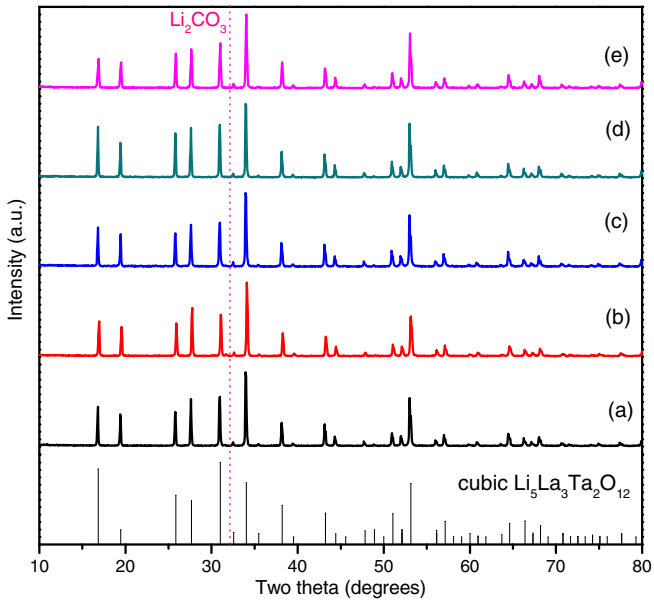

Figure 1. The powder X-ray diffraction (PXRD) patterns of $Li_6La_3Ta_{1.5}Y_{0.5}O_{12}$ prepared via solid state synthesis method with varying amounts of excess (a) 2.5, (b) 5, (c) 7, (d) 10 and (e) 15 wt. % $LiNO_3$ and a calculated pattern for cubic garnet ($Li_5La_3Ta_2O_{12}$ ICSD # 01-074-9856 where ICSD stands for Inorganic Crystal Structure Database). Expected peak for Li_2CO_3 is also marked with a dotted line at ~31.92° (JCPDS # 22-1141 where JCPDS stands for Joint Committee on Powder Diffraction Standards).

Cu-Kα radiation at the University of Calgary. The theoretical density (d) was calculated using the lattice parameter derived from PXRD analysis by employing the equation;

$$d = \frac{ZM}{a^3 N_A} \quad [1]$$

where Z, M, *a*, and N_A represent the number of chemical formula per unit cell (Z = 8 in the present Li-stuffed garnets), molar mass of the nominal chemical composition $Li_6La_3Ta_{1.5}Y_{0.5}O_{12}$, lattice parameter obtained from PXRD (Figure 1 and Table I), and Avogadro's number, respectively. Sample imaging was performed on a Hitachi SU-70 scanning electron microscope (SEM) at the University of Maryland. Micrometrics AccuPyc 1340, Gas Pycnometer was used to measure the density of $Li_6La_3Ta_{1.5}Y_{0.5}O_{12}$ powder samples in Calgary. Sample density was calculated based on mass (m) and volume (V_s) of the sample used in He displacement Pycnometer experiment, i.e.,

$$d = \frac{m}{V_s} \quad [2]$$

The term V_s depends on various factors such as the volumes of reference (V_r) and empty cell (V_c) and the gas pressure at different stages during the measurement, which can be represented as follows,

$$V_s = V_c - \frac{V_r}{\left(\frac{P_i - P_r}{P_f - P_r} - 1\right)} \quad [3]$$

where P_r, P_i, and P_f indicate the system reference, initial and final pressure, respectively. Raman spectroscopy was also performed with a 532 nm laser using a Horiba LabRAM ARAMIS Raman microscope at Maryland. The microscope settings used included a grating of 1800 mm^{-1} and a D1 filter (10 × intensity reduction). Results were measured between wavenumbers from 50 cm^{-1} to 1400 cm^{-1}.

At Calgary, Solartron SI 1260 impedance and gain-phase analyzer was used in the frequency range of 0.01 Hz to 6 MHz to determine the conductivity of the Li-stuffed garnets. The pellets were painted with Au electrodes and cured at 600°C for 1 h before conductivity measurements. The actual capacitance (C) values can be computed using the impedance data analysis as,

$$C = R^{\left(\frac{1-n}{n}\right)} CPE^{\left(\frac{1}{n}\right)} \quad [4]$$

where *R, CPE,* and *n* represent the resistance, constant phase element and the exponent which varies from 0 to 1. The total conductivity was determined using the formula,

$$\sigma = \left(\frac{1}{R}\right)\left(\frac{l}{a}\right) \quad [5]$$

where R is the resistance, *l* is the thickness of the sample and *a* is the area of the electrode.

Table I. Comparison of densities calculated from PXRD data and measured from He Pycnometer and the lattice parameter (*a*) of $Li_6La_3Ta_{1.5}Y_{0.5}O_{12}$ with excess amount of lithium (2.5 - 15 wt.% $LiNO_3$) added during solid-state synthesis.

Excess Li-salt (wt. %)	Theoretical density (gcm^{-3})	Measured density (gcm^{-3})	Lattice parameter, *a* (Å)	Density (%)
2.5	5.964	4.839(5)	12.911(1)	81
5	6.007	5.101(5)	12.880(3)	85
7	5.964	5.398(2)	12.911(1)	91
10	5.963	5.161(4)	12.912(1)	87
15	5.985	5.095(3)	12.896(1)	85

Results and Discussion

Structure and density.— Figure 1 shows the PXRD patterns of $Li_6La_3Ta_{1.5}Y_{0.5}O_{12}$ prepared using 2.5 to 15 wt. % excess $LiNO_3$ along with the calculated pattern for the cubic phase of $Li_5La_3Ta_2O_{12}$ (Inorganic Crystal Structure Database (ICSD) # 01-074-9856). PXRD show the formation of cubic phase in all the investigated $Li_6La_3Ta_{1.5}Y_{0.5}O_{12}$ samples. There is no secondary phase observed in the PXRD. It is found that the crystal structure is stable irrespective of the change in the amount of excess lithium content, which was added to avoid Li loss during high temperature sintering. The exact amount of Li in the investigated compound was unable to be quantified in the present study due to lack of available experimental method. However, there is no significant change in the cubic lattice constant as a function of Li content (Table I). The theoretical and measured density results of garnet-type $Li_6La_3Ta_{1.5}Y_{0.5}O_{12}$ prepared using 2.5 to 15 wt. % excess $LiNO_3$ obtained using PXRD and He pycnometer, respectively, are listed in Table I. The He pycnometer density was found to be in the range of 4.84–5.40 gcm^{-3} for $Li_6La_3Ta_{1.5}Y_{0.5}O_{12}$ prepared using 2.5 to 15 wt. % excess $LiNO_3$ (Table I), while the theoretical density obtained using XRD is ~ 6 gcm^{-3}. The density of the samples varied between 81 and 91%. The discrepancy in experimental density value can be attributed to the porosity of garnet oxides.

Microstructure and chemical composition.— Lithium dependence of microstructure is demonstrated by scanning electron microscopy (SEM) (Figure 2). The secondary electron images were recorded at different magnifications. Imaging was performed on slices of isostatically pressed pellets sintered at 1100°C for 6 h. Significant porosity is seen at the sample with 5 wt.% excess $LiNO_3$ and below, with a microstructure possibly indicating liquid phase sintering. This observation supports the lower density obtained from He Pycnometer (Table I). Grain growth generally increased from 7 to 15 wt.% excess $LiNO_3$, though 10 % excess $LiNO_3$ was out of the trend with somewhat smaller particle size. In general, the inter-particle contact decreased with increased excess $LiNO_3$, while the extent of grain growth increased. The beneficial impact of excess $LiNO_3$ on grain growth may have to be balanced with the lessened inter-particle contact. It seems that 7 wt. % excess $LiNO_3$ is close to this balancing point. Also, less

Downloaded on 2016-08-30 to IP 136.159.160.69 address. Redistribution subject to ECS terms of use (see ecsdl.org/site/terms_use) unless CC License in place (see abstract).

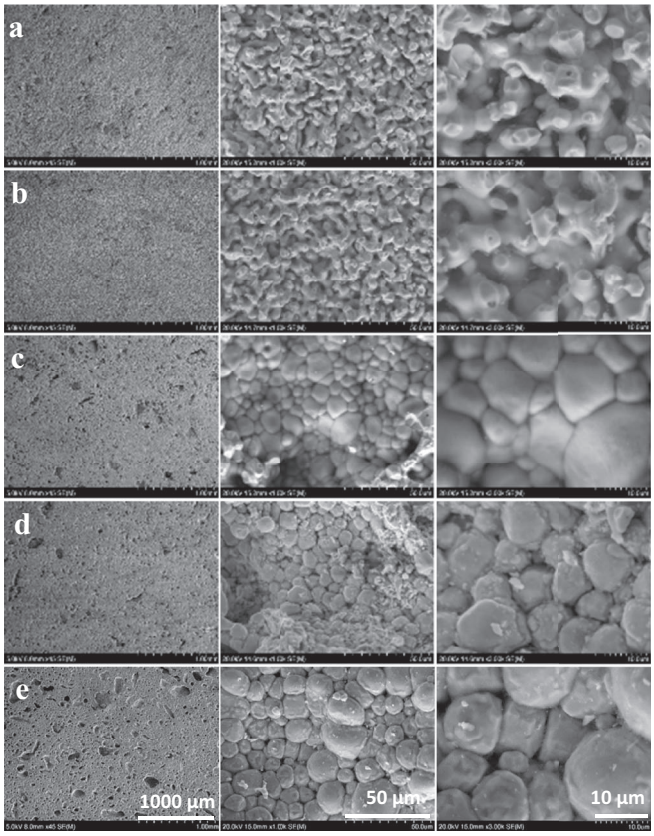

Figure 2. Scanning electron micrographs of $Li_6La_3Ta_{1.5}Y_{0.5}O_{12}$ with varying amounts of excess (a) 2.5, (b) 5, (c) 7, (d) 10, and (e) 15 wt. % $LiNO_3$ (corresponding higher magnification images are shown in the same row).

porosity with inter-particle contact and maximum density of 5.4 gcm^{-3} was observed for 7 wt. % $LiNO_3$ excess sample compared to others (Table I).

The elemental distribution (EDS mapping) of $Li_6La_3Ta_{1.5}Y_{0.5}O_{12}$ prepared using 2.5 to 15 wt. % excess $LiNO_3$ is shown in Figure 3, indicating the presence of heavy elements in the composition along with the Al contamination from the crucible used for the synthesis. The EDS mapping further indicates that there is no significant segregation of Al or other elements in $Li_6La_3Ta_{1.5}Y_{0.5}O_{12}$ prepared using 2.5 to 15 wt. %. The presence of Al contamination was further confirmed from the ^{27}Al MAS NMR studies, as shown in Figure 4. The peak close to 0 ppm indicates the octahedral coordination of Al, while the other peak close to 70 ppm indicates the tetrahedral coordination of Al.[8,16,22–24] Geiger et al. proposed that the octahedral sites occupied by Al^{3+} could lead to distortion.[25] It is possible that Al^{3+} substitutes for Li^+ sites and creates lithium vacancies in the structure which affect the structural stabilization.[26] $Li_7La_3Zr_2O_{12}$ garnet needs a critical concentration of 0.204 moles of Al to stabilize cubic structure and it exists as tetragonal polymorph below that concentration limit.[26] Though EDS mapping showed no significant segregation of Al at grain boundaries in this study, a small amount of Al could also be present at grain-boundaries as an amorphous phase, which acts as sintering aid and prevents Li volatilization during sintering.[27] There was no indication of aluminum containing impurity peaks in PXRD (Figure 1), which could be due to the detection limit of the technique. Chemical shift value of ^7Li MAS NMR was reported against LiCl standard (Figure 5). In all the cases, a single peak was obtained close to 0 ppm which is typical for Li-stuffed garnet-type oxides.[7,8,16,28]

Raman spectroscopy.— Raman spectroscopy was performed to reveal the presence of any surface phases and fingerprint the garnet phase. Figure 6 shows that the spectrograph matches that of cubic garnet regardless of excess lithium amount.[29,30] However, it is also apparent that all samples show some amount of Li_2CO_3 formation on

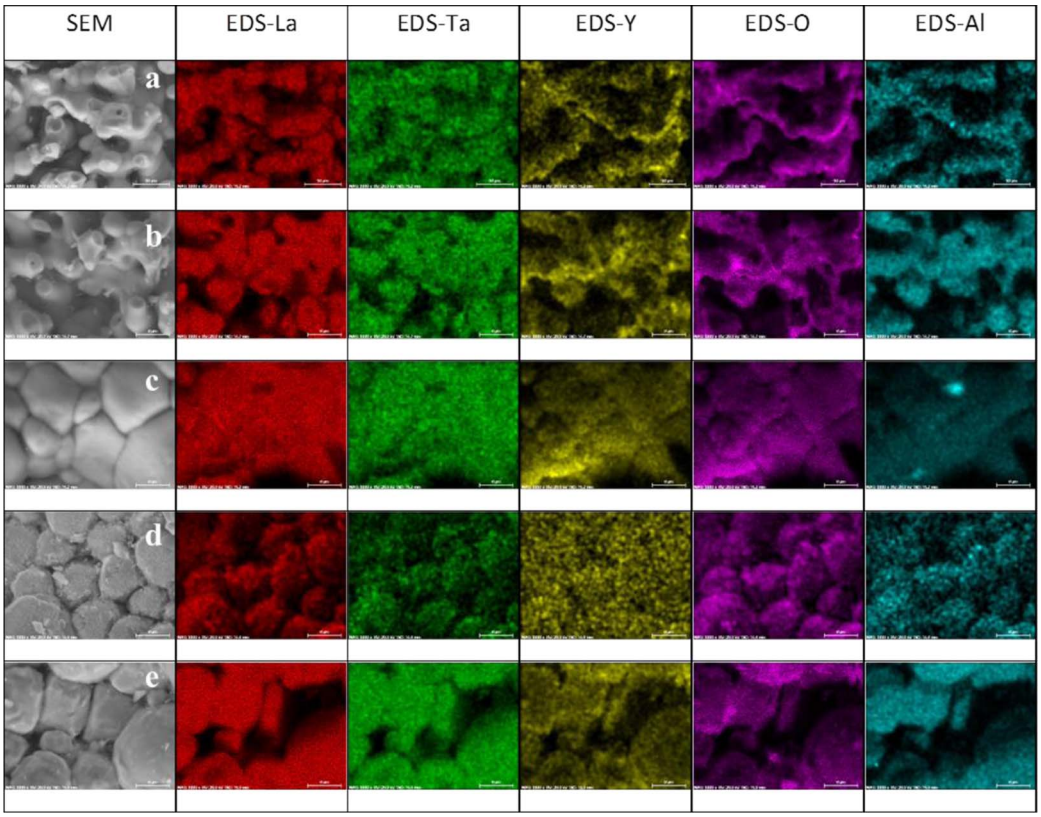

Figure 3. SEM image and corresponding elemental mapping of $Li_6La_3Ta_{1.5}Y_{0.5}O_{12}$ with varying amounts of excess (a) 2.5, (b) 5, (c) 7, (d) 10 and (e) 15 wt. % $LiNO_3$.

Downloaded on 2016-08-30 to IP 136.159.160.69 address. Redistribution subject to ECS terms of use (see ecsdl.org/site/terms_use) unless CC License in place (see abstract).

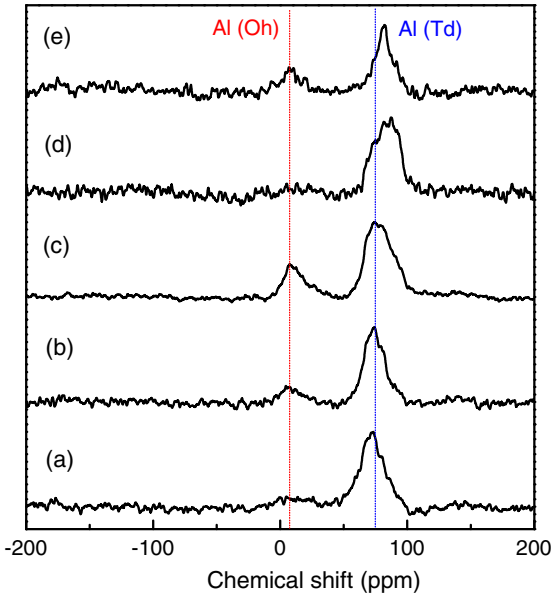

Figure 4. ^{27}Al MAS NMR of $Li_6La_3Ta_{1.5}Y_{0.5}O_{12}$ with varying amounts of excess (a) 2.5, (b) 5, (c) 7, (d) 10, and (e) 15 wt. % $LiNO_3$ measured against $Al(NO_3)_3$ as standard.

the surface, as evidenced by the strong peak at 1090 cm^{-1}. However, the expected carbonate peak ($2\theta \sim 31.92°$, JCPDS # 22-1141 where JCPDS stands for Joint Committee on Powder Diffraction Standards) is not present in PXRD patterns (Figure 1). The detection of Li_2CO_3 in Raman, but not in PXRD, signifies that the Li_2CO_3 is likely a minority phase existing as a surface layer formed in a reaction between lithium garnet and atmospheric CO_2. The presence of Li_2CO_3 due to the sample exposure to atmosphere is also reported recently using the techniques such as X-ray photoelectron spectroscopy (XPS) and soft X-ray absorption spectroscopy (sXAS).[31] There is no correlation between excess lithium in the sample and intensity of the Raman peak signifying Li_2CO_3. The samples may have had slightly different exposures to the atmosphere. Lithium vibrations are expected between 300 and

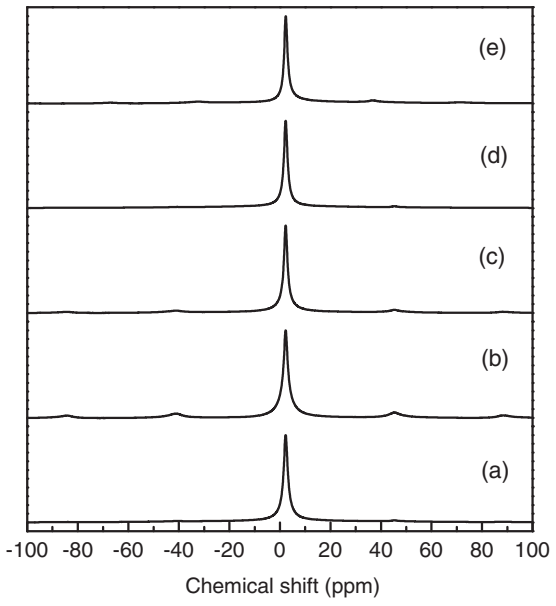

Figure 5. ^{7}Li MAS NMR of $Li_6La_3Ta_{1.5}Y_{0.5}O_{12}$ with varying amounts of excess (a) 2.5, (b) 5, (c) 7, (d) 10, and (e) 15 wt. % $LiNO_3$. The standard material used was LiCl.

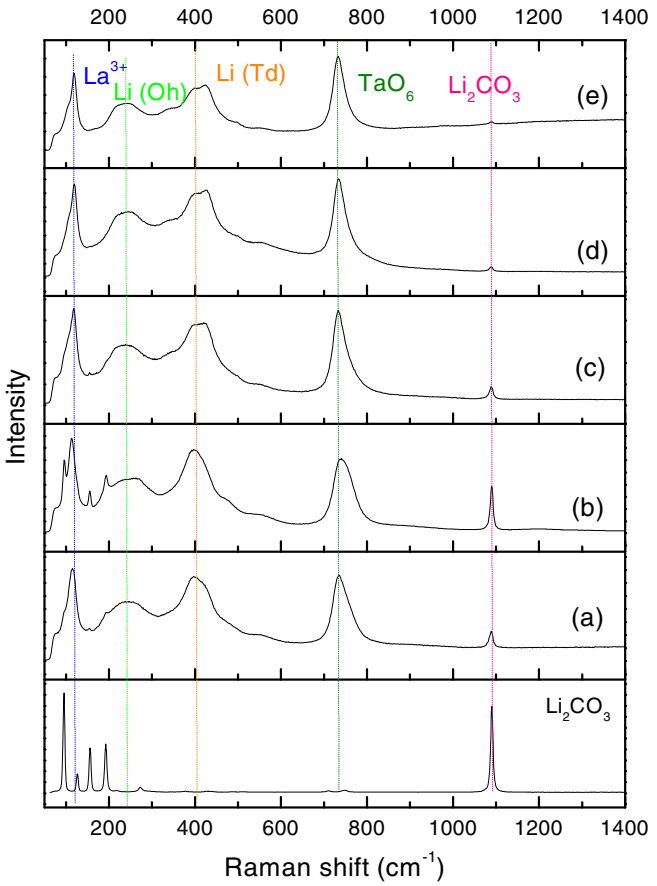

Figure 6. Raman spectroscopy of $Li_6La_3Ta_{1.5}Y_{0.5}O_{12}$ with varying amounts of excess (a) 2.5, (b) 5, (c) 7, (d) 10 and (e) 15 wt. % $LiNO_3$. For comparison, Raman spectrum of commercial Li_2CO_3 is also shown.

600 cm^{-1}, more specifically in Figure 6, the internal modes of octahedrally coordinated lithium occur at 200–300 cm^{-1} and that of tetrahedrally coordinated lithium occur at 350–600 cm^{-1}.[18,32] The peak at $\sim$750 cm^{-1} could be due to the stretching modes of TaO_6 octahedra.[33]

Electrical conductivity.— Typical AC impedance spectra of $Li_6La_3Ta_{1.5}Y_{0.5}O_{12}$ prepared using 2.5 to 15 wt. % excess $LiNO_3$ recorded in air at 50°C are shown in Figure 7, and the equivalent circuit used for fitting are shown as inset figures. Two semicircles and a spike due to lithium ion blocking electrodes are seen for 2.5 wt.% excess sample, and two sets of parallel resistor-capacitor and a series capacitor was used for the fitting (Figure 7a). Only one semicircle and a spike is seen in case of Figures 7b and 7c. The fitting results are provided in Table II and the capacitance values show that the conductivity contributions are from the bulk and grain-boundaries. The shape of impedance spectra shows the typical behavior of garnet-type oxides.[18,19]

Figure 8 shows the Arrhenius plots for bulk Li ion conductivity of the $Li_6La_3Ta_{1.5}Y_{0.5}O_{12}$ prepared with varying excess of $LiNO_3$. The maximum conductivity obtained is for the 10 and 15 wt. % $LiNO_3$ excess samples and a drop in conductivity of couple of orders of magnitude was observed for all other cases (2.5 to 7 wt. %). The conductivity obtained for 10 wt. % Li sample is 1.62×10^{-4} Scm^{-1} at 24°C, while a lower conductivity of 3.78×10^{-6} Scm^{-1} was found for the least conductive sample, with 2.5 wt.% $LiNO_3$ excess. The activation energy was obtained by employing the Arrhenius equation (Equation 6),

$$\sigma T = A \exp^{\left(-\frac{E_a}{kT}\right)} \quad [6]$$

Downloaded on 2016-08-30 to IP 136.159.160.69 address. Redistribution subject to ECS terms of use (see ecsdl.org/site/terms_use) unless CC License in place (see abstract).

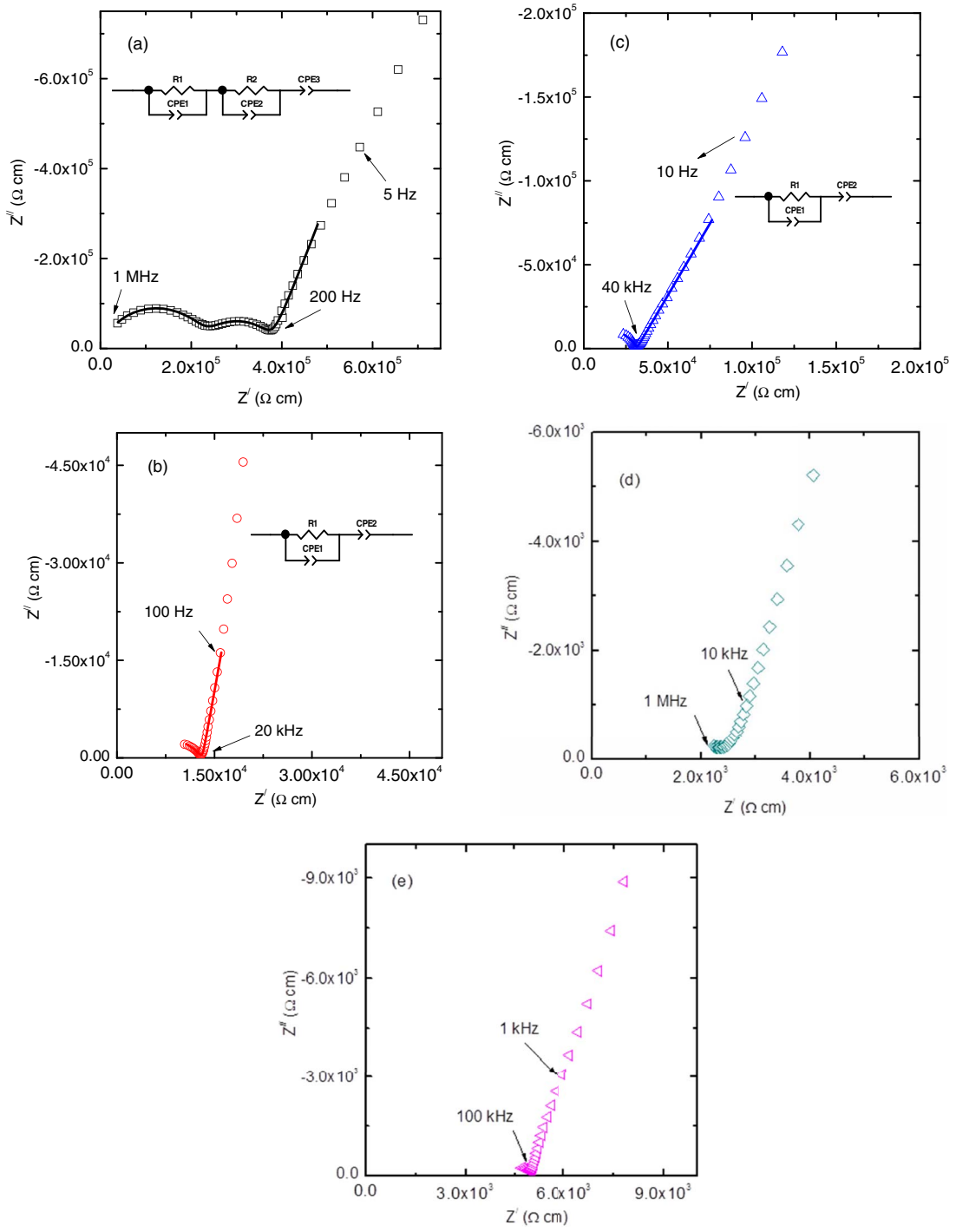

Figure 7. Typical AC impedance spectra of $Li_6La_3Ta_{1.5}Y_{0.5}O_{12}$ with varying amounts of excess (a) 2.5, (b) 5, (c) 7, (d) 10, and (e) 15 wt. % $LiNO_3$ measured in air at 50°C. The open symbols and solid lines represent the measured and fitted data, respectively. The equivalent circuit used to fit the impedance data of 2.5 and 5 and 7 wt. % $LiNO_3$ members is shown in the inset figure.

Table II. The AC impedance fitting results measured at 50°C of $Li_6La_3Ta_{1.5}Y_{0.5}O_{12}$ with excess amount of lithium (2.5, 5 and 7 wt. % $LiNO_3$) added during solid-state synthesis.

Excess Li-salt (wt. %)	R_b (Ω)	CPE_b (F)	n	C_b (F)	n	CPE_{gb} (F)	C_{gb} (F)	CPE_{el} (F)	χ^2
2.5	4.93×10^4	1.98×10^{-10}	0.81	1.24×10^{-11}	0.81	1.35×10^{-8}	2.02×10^{-9}	6.75×10^{-7}	3×10^{-4}
5	2.97×10^3	1.34×10^{-8}	0.57	6.79×10^{-12}	-	-	-	6.63×10^{-7}	2×10^{-4}
7	8.18×10^3	5.30×10^{-10}	0.74	6.32×10^{-12}	-	-	-	2.05×10^{-6}	4×10^{-4}

Downloaded on 2016-08-30 to IP 136.159.160.69 address. Redistribution subject to ECS terms of use (see ecsdl.org/site/terms_use) unless CC License in place (see abstract).

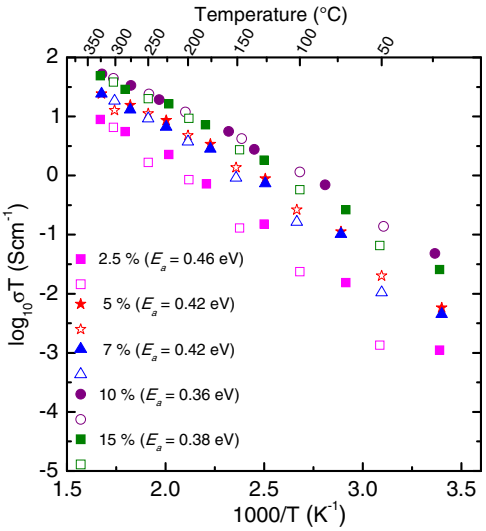

Figure 8. The Arrhenius plots of $Li_6La_3Ta_{1.5}Y_{0.5}O_{12}$ (2.5 – 15 wt.% excess $LiNO_3$) showing the bulk Li ion conductivity as a function of temperature. The closed and open symbols represent the heating and cooling cycles, respectively.

where A is the pre-exponential factor, E_a is the activation energy, T is the temperature, and k is the Boltzmann constant (1.38×10^{-23} JK^{-1}). The higher conductivity samples show a decrease in activation energy over the temperature range of 24–325°C, as shown in Figure 8. This can be attributed due to the fact that the excess $LiNO_3$ added during synthesis acts as a sintering aid, which increases the grain-to-grain contact and also decreases the grain-boundary resistance. A comparison graph of calculated and measured densities from PXRD data using the PROSZKI program and He Pycnometry respectively, along with activation energy as a function of different excess Li content of $Li_6La_3Ta_{1.5}Y_{0.5}O_{12}$ (2.5–15 wt. % excess $LiNO_3$) is shown in Figure 9. It is noticeable that with the increase in measured density, activation energy tends to decrease, indicating that the excess Li salt has a positive role in increasing the density of the investigated Li-stuffed $Li_6La_3Ta_{1.5}Y_{0.5}O_{12}$.

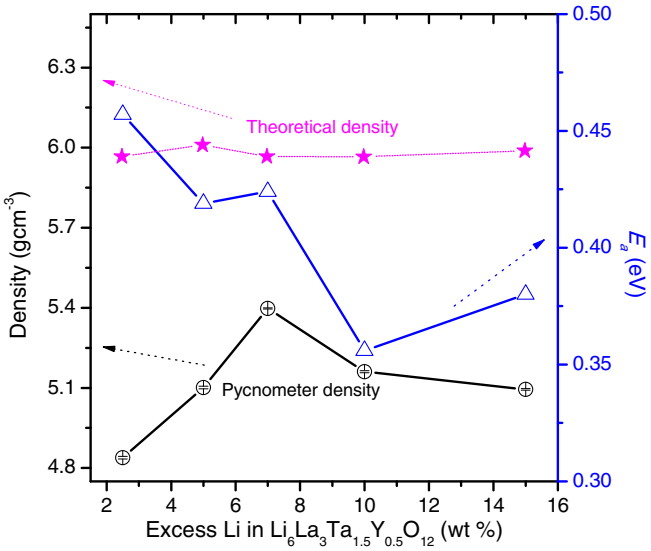

Figure 9. Correlation of density and activation energy (calculated at 24–325°C) with the excess $LiNO_3$ wt. % (2.5 – 15 wt.%) used for the synthesis of $Li_6La_3Ta_{1.5}Y_{0.5}O_{12}$. It shows that the activation energy decreases with increase in density of the ceramics.

Conclusions

This study sheds some light on the role of excess lithium in the synthesis of lithium garnets. $Li_6La_3Ta_{1.5}Y_{0.5}O_{12}$ was produced with varying excess amounts of $LiNO_3$ and characterized by powder X-ray diffraction, scanning electron microscopy, AC impedance and Raman spectroscopy. The desired cubic phase was obtained for all the compositions and the lattice parameter was essentially constant irrespective of the amount of excess lithium in the composition. The amount of excess lithium had an insignificant effect on the lattice structure or propensity to develop lithium carbonates in air, but sinterability and conductivity showed clear maxima in the range tested. $Li_6La_3Ta_{1.5}Y_{0.5}O_{12}$ with 10 and 2.5 wt. % excess Li showed the highest and lowest conductivity of 1.62×10^{-4} Scm^{-1} and 3.77×10^{-6} respectively, at 24°C among all other members. This study shows that the optimization of excess $LiNO_3$ addition can dramatically improve the properties of final sintered Li-stuffed garnets.

Acknowledgments

This work was performed with financial support from the US Department of Energy ARPA-E RANGE contract #DE-AR0000384.

References

1. V. Thangadurai, S. Narayanan, and D. Pinzaru, *Chem. Soc. Rev.*, **43**, 4714 (2014).
2. V. Thangadurai, D. Pinzaru, S. Narayanan, and A. K. Baral, *J. Phys. Chem. Lett.*, **6** 292 (2015).
3. R. Murugan, V. Thangadurai, and W. Weppner, *Angew. Chem. Int. Ed. Engl.*, **46**, 7778 (2007).
4. J. Awaka, N. Kijima, H. Hayakawa, and J. Akimoto, *J. Solid State Chem.*, **182**, 2046 (2009).
5. V. Thangadurai, H. Kaack, and W. J. F. Weppner, *J. Am. Ceram. Soc.*, **86**, 437 (2003).
6. V. Thangadurai and W. Weppner, *J. Solid State Chem.*, **179**, 974 (2006).
7. S. Narayanan and V. Thangadurai, *J. Power Sources*, **196**, 8085 (2011).
8. S. Narayanan, F. Ramezanipour, and V. Thangadurai, *J. Phys. Chem. C*, **116**, 20154 (2012).
9. V. Thangadurai and W. Weppner, *Adv. Funct. Mater.*, **15**, 107 (2005).
10. Y. Li, C.-A. Wang, H. Xie, J. Cheng, and J. B. Goodenough, *Electrochem. Comm.*, **13**, 1289 (2011).
11. L. Cheng, J. S. Park, H. Hou, V. Zorba, G. Chen, T. Richardson, J. Cabana, R. Russo, and M. Doeff, *J. Mater. Chem. A*, **2**, 172 (2014).
12. H. Peng, Q. Wu, and L. Xiao, *J. Sol-Gel Sci. Technol.*, **66**, 175 (2013).
13. K. Tadanaga, R. Takano, T. Ichinose, S. Mori, A. Hayashi, and M. Tatsumisago, *Electrochem. Comm.*, **33**, 51 (2013).
14. R. Takano, K. Tadanaga, A. Hayashi, and M. Tatsumisago, *Solid State Ionics*, **255**, 104 (2014).
15. H. Buschmann, J. Dolle, S. Berendts, A. Kuhn, P. Bottke, M. Wilkening, P. Heitjans, A. Senyshyn, H. Ehrenberg, A. Lotnyk, V. Duppel, L. Kienle, and J. Janek, *Phys. Chem. Chem. Phys.*, **13**, 19378 (2011).
16. C. A. Geiger, E. Alekseev, B. Lazic, M. Fisch, T. Armbruster, R. Langner, M. Fechtelkord, N. Kim, T. Pettke, and W. Weppner, *Inorg. Chem.*, **50**, 1089 (2011).
17. J. H. Ahn, S.-Y. Park, J.-M. Lee, Y. Park, and J.-H. Lee, *J. Power Sources*, **254**, 287 (2014).
18. N. Janani, C. Deviannapoorani, L. Dhivya, and R. Murugan, *RSC Advances*, **4**, 51228 (2014).
19. K. Liu, J.-T. Ma, and C.-A. Wang, *J. Power Sources*, **260**, 109 (2014).
20. Y. Li, Y. Cao, and X. Guo, *Solid State Ionics*, **253**, 76 (2013).
21. J. E. Ni, E. D. Case, J. S. Sakamoto, E. Rangasamy, and J. B. Wolfenstine, *J. Mater. Sci.*, **47**, 7978 (2012).
22. S. Narayanan, V. Epp, M. Wilkening, and V. Thangadurai, *RSC Advances*, **2**, 2553 (2012).
23. S. Narayanan and V. Thangadurai, *J. Power Sources*, **196**, 8085 (2011).
24. B. Koch and M. Vogel, *Solid State Nucl. Magn. Reson.*, **34**, 37 (2008).
25. H. Xie, J. A. Alonso, Y. Li, M. T. Fernández-Díaz, and J. B. Goodenough, *Chem. Mater.*, **23**, 3587 (2011).
26. E. Rangasamy, J. Wolfenstine, and J. Sakamoto, *Solid State Ionics*, **206**, 28 (2012).
27. Y. Li, J.-T. Han, C.-A. Wang, H. Xie, and J. B. Goodenough, *J. Mater. Chem.*, **22**, 15357 (2012).
28. C. Bernuy-Lopez, W. Manalastas, J. M. Lopez del Amo, A. Aguadero, F. Aguesse, and J. A. Kilner, *Chem. Mater.*, **26**, 3610 (2014).
29. F. Tietz, T. Wegener, M. T. Gerhards, M. Giarola, and G. Mariotto, *Solid State Ionics*, **230**, 77 (2013).
30. G. T. Hitz, E. D. Wachsman, and V. Thangadurai, *J. Electrochem. Soc.*, **160**, A1248 (2013).
31. L. Cheng, E. J. Crumlin, W. Chen, R. Qiao, H. Hou, S. F. Lux, V. Zorba, R. Russo, R. Kostecki, Z. Liu, K. Persson, W. Yang, J. Cabana, T. Richardson, G. Chena, and M. Doeff, *Phys. Chem. Chem. Phys.*, **16**, 18294 (2014).
32. G. Larraz, A. Orera, and M. L. Sanjuán, *J. Mater. Chem. A*, **1**, 11419 (2013).
33. T. Thompson, J. Wolfenstine, J. L. Allen, M. Johannes, A. Huq, I. N. Davida, and J. Sakamoto, *J. Mater. Chem. A*, **2**, 13431 (2014).

Downloaded on 2016-08-30 to IP 136.159.160.69 address. Redistribution subject to ECS terms of use (see ecsdl.org/site/terms_use) unless CC License in place (see abstract).